

Microfluidic switch based on combined effect of hydrodynamics and electroosmosis

Haiwang Li · Teck Neng Wong · Nam-Trung Nguyen

Received: 30 July 2010 / Accepted: 20 October 2010 / Published online: 9 November 2010
© Springer-Verlag 2010

Abstract This paper presents theoretical and experimental investigations on valveless microfluidic switch using the coupled effect of hydrodynamics and electroosmosis. Switching of a non-conducting fluid stream is demonstrated. The first part of the investigation focused on flow switching of a non-conducting fluid, while the second part focused on switching of aqueous liquid droplets in a continuous oil stream. Two sheath streams (aqueous NaCl and glycerol) and a sample stream (silicon oil) are introduced by syringe pumps to flow side by side in a straight rectangular microchannel. External electric fields are applied on the two sheath streams. The switching process using electroosmotic effect for different flow rate and viscosity of sample stream is investigated. The results indicate that the switching response time is affected by the electric fields, flow rate, and viscosity of the sample. At constant inlet volumetric flow rates, the sample streams or droplets can be delivered to the desired outlet ports using applied voltages.

Keywords Microchannel · Switch · Sample flow · Droplets · Electroosmosis

List of symbols

e_1, e_2, e_3 Liquid fractions
 e Elementary charge, $e = 1.602 \times 10^{-9}$ (C)
 E_x The electric field
G Parameter measuring the electroosmotic force by external electric field

h Height of the microchannel (m)
 L_{ref} The length scale
 M Electrokinetic effect in the matching conditions
 n_0 Ionic number concentration in the bulk (m^{-3})
 n_i Ionic number concentration of the type i in the bulk (m^{-3})
 k_b Boltzmann constant, $k = 1.381 \times 10^{-23}$ (J K^{-1})
 K Electrokinetic parameter
 p Pressure
 q Flowrate
 \mathbf{r} Position vector (m)
 Re Reynolds number
 t Time (s)
 T Temperature (K)
 u Velocity
 U_{ref} The velocity scale
 V Voltage
 w Half of width of the channel (m)
 z_0 The valence of the ions

Greek symbols

ρ Density
 ψ_0 Electrostatic potential
 ξ Zeta potential
 ε The permittivity of the dielectric
 ε_0 The permittivity of the dielectric of vacuum
 ε_r The dielectric constant comparing with ε_0
 ψ The electric potential
 μ Dynamic viscosity
 κ Debye–Hückel parameter (m^{-1})
 ρ_q^s The surface charge density
 β Dynamic viscosity ratios

Subscripts

ref Reference quantity

H. Li · T. N. Wong (✉) · N.-T. Nguyen
School of Mechanical and Aerospace Engineering,
Nanyang Technological University, 50 Nanyang Avenue,
Singapore 639798, Singapore
e-mail: mtnwong@ntu.edu.sg

- 1 Conducting fluid 1
- 2 Non-conducting fluid 2
- 3 Conducting fluid 3
- q Charge of bulk

Superscripts

- 0 Fundamental state
- Dimensionless parameter
- p Pressure driven
- E Electroosmotic effect
- ' Derivative
- I Integrate

Operators

- ∇ Gradient
- $\hat{\partial}$ Partial differential

1 Introduction

Microfluidics has been the key technology for lab on a chip (LOC). Microfluidic devices have several inherent advantages in LOC applications. The main advantages are small device size, low fabrication cost, small sample size, low energy consumption, and the high surface to volume ratio (Andersson and Van den Berg 2003; Stone et al. 2004; Dittrich and Manz 2005; Huh et al. 2005). Many LOC applications require valveless flow switching and focusing as the initial step. Examples are cell handling and analysis, clinical diagnosis, immunoassays, DNA and proteins processing, environmental concerns and gas analysis, and others (Dittrich et al. 2006). Furthermore, switching and sorting droplets are important techniques in the fields of fine chemical or pharmaceutical engineering. The method for separating droplets is the alternative to direct production of monodisperse emulsions (Maenaka et al. 2008). As a result, research and development on flow and droplet switching have attracted a great interest from the microfluidics research community.

The main switching techniques in microfluidics are hydrodynamic and electrokinetic switching. The hydrodynamic technique generally involves the use of unbalanced hydrodynamically driven sheath streams to direct the sample stream to the desired outlet ports. Comparing with hydrodynamic switching, electrokinetic switching involves electroosmotic flow and has some distinct advantages. For example, electroosmotic flow has a uniform velocity profile; the velocity of electroosmotic flow is easier to be predicted. Furthermore, high speed flow switching required for dynamic particle separation is easily implemented using electroosmotic concept (Huh et al. 2005; Taylor et al. 2008).

Besselink et al. (2004) controlled the position and width of a sample stream in a chamber using a valveless and electroosmotically driven technique. Controlling the sheath flow using electric fields can position the sample stream accurately. Similar to the work of Besselink et al. (2004), Kohlheyer et al. (2005) controlled the position and width of two sample streams in a chamber using electroosmotically driven flow. Fu et al. (2004) designed an innovative micro flow cytometer, which focuses and switches the sample stream using electroosmosis. Fu et al. (2003) experimentally investigated the use of electrokinetic force to control the fluid flow for bio-analytical applications in different microfluidic chips. A new control model for ‘one-to-multiple’ electrokinetically pre-focused micro flow switches were proposed by Yang et al. (2005). Using this model, the sample stream can be pre-focused and injected into the desired outlets electroosmotically. By applying the minimum number of voltage control points, Pan et al. (2006) electroosmotically switched the sample stream to the desired outlets for bio-analytical applications. Applying a simple voltage control model to the inlet and outlet ports, Pan et al. (2007) combined focusing and electroosmotic switching for mixing enhancement. Taylor et al. (2008) reported a microfluidic switch for sorting using electroosmosis. The response time is an important parameter for switching techniques. Wolfe et al. (2004) reported switching with a response time of 2 s. The response time reported by Campbell et al. (2004) was 20 ms. Hydrodynamic switching reported by Nguyen et al. (2007) has a response time of 0.3 s.

Tan and Lee (2005) and Huh et al. (2007) reported that microfluidic devices can be used to separate droplets using hydrodynamic effect. A cell counting and sorting system which can be used as cytometer was designed by Yang et al. (2006), the cell can be sorted at a frequency of 120 cells min^{-1} . Lin and Lee (2003), Lee et al. (2005), and Ateya et al. (2008) designed microfluidic cytometers for cell counting and sorting. Beside the hydrodynamic effect, other effects can also be used to sort liquid droplets. For example, Braschler et al. (2008) reported a particle-sorting device based on dielectrophoresis.

Although electroosmotic effect is an effective method for valveless switching, this concept has some drawbacks for the use in purely electrokinetically driven systems. First, the flow is unstable if the electric field is too high arising from the conductivity mismatch and strong electric field (Chen and Santiago 2002a; Lin et al. 2004; Chen et al. 2005). Second, particles are exposed to Joule heating under the applied electric field. If the electric field is too strong, the particles can be damaged due to induced heat (McClain et al. 2001). To overcome the drawback of the electrokinetically driven systems, we combine the hydrodynamic

effect and the electroosmotic effect for switching applications.

This paper consists of three parts. The first part presents an analytical model of three-fluid flow in a rectangular microchannel under the coupled effects of electroosmosis and hydrodynamics. Using the Newton–Raphson method, the liquid fractions of three fluids are obtained. The second part presents experimental results of valveless flow switching in a Y-shaped polydimethylsiloxane (PDMS) microchannel under the coupled effect of pressure driven and electroosmotic flows. Figure 1a shows schematically the microchannel system used for flow switching of a non-conducting sample stream. Liquid fractions are investigated by fluorescence imaging technique. Experimental results are compared to the analytical solutions. The last part presents droplet switching in a T-shaped polymethylmethacrylate (PMMA) microchannel under the coupled effect of pressure driven and electroosmotic flows. Figure 1b shows flow switching with droplet generation in the non-conducting stream. Generation of these water droplets can be achieved by shearing the water stream at a T-junction by a continuous mineral oil stream.

2 Mathematical model

The details of the mathematical model are provided by our previous work (Haiwang et al. 2009). Figure 1c shows the model of valveless flow switching in a Y-shaped microchannel using coupled hydrodynamics and electroosmosis. The microchannel system consists of three inlets (I_1 – I_3) and five outlets (O_1 – O_5). In this paper, the non-polar liquids with low conductivity ($<10^{-6} \text{ Sm}^{-1}$), such as oil, cannot form the necessary double layer and therefore can be regarded as non-conducting fluid (Chen and Santiago 2002b; Brask et al. 2005). Polar liquids with high conductivity ($>10^{-6} \text{ Sm}^{-1}$), such as aqueous salt, can form the necessary double layer and therefore are regarded as conducting fluid. Two sheath streams (fluid 1 and fluid 3) are electrically conducting with high electroosmotic mobility, while the focused stream (fluid 2) is non-conducting with low electroosmotic mobility. Fluids 1 and 3 are immiscible to fluid 2. Due to the relatively small channel height, the interfaces between the fluids are assumed as flat. The liquids fill the entire height of the channel. Inertial effects are negligible. At a given pressure gradient and electric fields applied along the conducting sheath streams, electroosmotic forces control the widths of fluid streams. The widths of the sheath streams depend on the directions and magnitudes of the applied electric fields. The fluid with low electroosmotic mobility is focused and switched to the desired outlet ports by the interfacial forces of the conducting fluids as well as by the pressure gradient. The

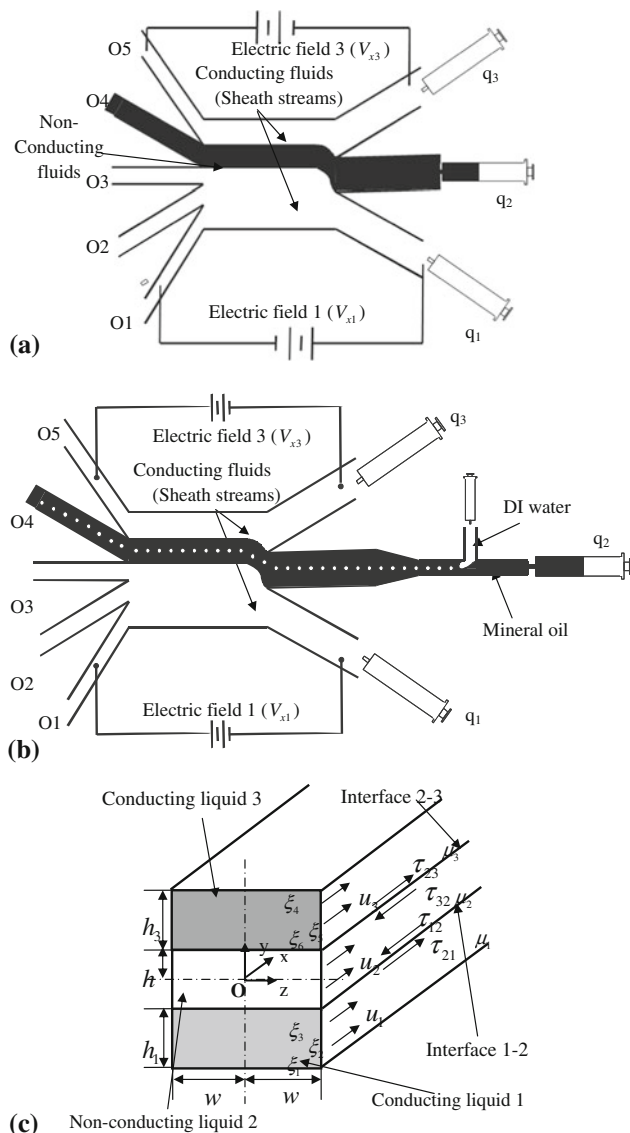


Fig. 1 Schematic representation of three-fluid electroosmotic switching: **a** switching without droplets, **b** switching with droplets, **c** cross-sectional view of the model

electric potentials in the conducting fluids due to the charged walls are ψ_1 and ψ_3 , respectively. The reference length and the reference velocity of the flow are taken as $L_{ref} = (h_1 + 2h + h_3)/2$ and $U_{ref} = (E_{x1}\epsilon_0\epsilon_r k_b T)/(\mu_{ref} z_0)$, respectively. The independent position vector \mathbf{r} and dependent variables such as velocity u , pressure p , potential ψ , and density ρ_q are expressed in terms of corresponding dimensionless quantities (shown with an overbar):

$$\begin{cases} \mathbf{r} = L_{ref} \bar{\mathbf{r}} \\ u = U_{ref} \bar{u} \\ \psi = k_b T \bar{\psi} / (z_0 e) \\ p = \rho_{ref} U_{ref}^2 \bar{p} \\ \rho_q = 2n_0 z_0 e \bar{\rho}_q \end{cases} \quad (1)$$

The position vector \mathbf{r} includes thickness of the channel (h_i) and width of the channel (w), k_b is Boltzmann constant, T is the absolute temperature, z_0 is the valence of the ions, e is elementary charge, and n_0 is the reference value of the ion concentration, ϵ_r is the relative permittivity of the conducting fluids, and ϵ_0 is the permittivity of vacuum.

In the theoretical model, the electric potentials in the sheath streams (conducting fluid) are described by the Poisson-Boltzmann equation as

$$\text{(conducting fluid 1)} \quad \nabla^2 \bar{\psi}_1 = K^2 \bar{\psi}_1 \tag{2}$$

$$\text{(conducting fluid 3)} \quad \nabla^2 \bar{\psi}_3 = K^2 \bar{\psi}_3 \tag{3}$$

where $K = L_{\text{ref}} \kappa$, κ is the Debye–Hückel parameter,

$$\frac{1}{\kappa} = \left(\frac{\epsilon k_b T}{2z_0^2 e^2 n_0} \right)^{\frac{1}{2}} \tag{4}$$

The momentum equations for sheath streams (conducting fluids) and sample stream (non-conducting fluid) are

$$\text{(conducting fluid 1)} \quad \frac{\partial^2 \bar{u}_1}{\partial \bar{y}^2} + \frac{\partial^2 \bar{u}_1}{\partial \bar{z}^2} = Re \frac{d\bar{p}}{d\bar{x}} - Re G_{x1} \bar{\rho}_{q1} \tag{5}$$

$$\text{(non-conducting fluid 2)} \quad \frac{\partial^2 \bar{u}_2}{\partial \bar{y}^2} + \frac{\partial^2 \bar{u}_2}{\partial \bar{z}^2} = \frac{Re d\bar{p}}{\beta_2 d\bar{x}} \tag{6}$$

$$\text{(conducting fluid 3)} \quad \frac{\partial^2 \bar{u}_3}{\partial \bar{y}^2} + \frac{\partial^2 \bar{u}_3}{\partial \bar{z}^2} = \frac{Re d\bar{p}}{\beta_3 d\bar{x}} - Re G_{x3} \bar{\rho}_{q3} \tag{7}$$

where $\beta_2 = \mu_2/\mu_1$, $\beta_3 = \mu_3/\mu_1$, $G_{x1} = (2z_0 e n_0 L_{\text{ref}} V_{x1})/\rho_{\text{ref}} U_{\text{ref}}^2$, $G_{x3} = (2z_0 e n_0 L_{\text{ref}} V_{x3})/\rho_{\text{ref}} U_{\text{ref}}^2$.

No-slip boundary conditions are applied at the channel walls. In addition, the matching conditions at the interfaces such as continuity of velocities and force balance are applied.

The continuity conditions of the velocities at the liquid–liquid interfaces are:

$$\bar{u}_1 = \bar{u}_2, \quad \text{at } \bar{y} = -\bar{h} \quad (\text{interface 1–2}) \tag{8}$$

$$\bar{u}_2 = \bar{u}_3, \quad \text{at } \bar{y} = \bar{h} \quad (\text{interface 2–3}) \tag{9}$$

The shear stress balances that jump abruptly at the interface due to the presence of surface charge are

$$\frac{\partial \bar{u}_1}{\partial \bar{y}} + M_1 \bar{\rho}_{q1}^s = \beta_2 \frac{\partial \bar{u}_2}{\partial \bar{y}}, \quad \text{at } \bar{y} = -\bar{h} \quad (\text{interface 1–2}) \tag{10}$$

$$\beta_3 \frac{\partial \bar{u}_3}{\partial \bar{y}} + M_3 \bar{\rho}_{q3}^s = \beta_2 \frac{\partial \bar{u}_2}{\partial \bar{y}}, \quad \text{at } \bar{y} = \bar{h} \quad (\text{interface 2–3}) \tag{11}$$

where $M_1 = (\epsilon k_b T V_{x1})/(z_0 e U_{\text{ref}} \mu_{\text{ref}})$ and $M_3 = (\epsilon k_b T V_{x3})/(z_0 e U_{\text{ref}} \mu_{\text{ref}})$. In Eq. 10, $\bar{\mu}_1 \frac{\partial \bar{u}_1}{\partial \bar{y}}$ is the shear stress of fluid 1

at the interface 1–2; $\bar{\mu}_2 \frac{\partial \bar{u}_2}{\partial \bar{y}}$ is the shear stress of fluid 2 at the interface 1–2; M_1 is the dimensionless electrical force at interface 1–2; $\bar{\rho}_{q1}^s$ is the dimensionless density of surface charge at the interface 1–2, these values can be calculated according interface zeta potential (Gao et al. 2007; Li et al. 2009); $M_1 \bar{\rho}_{q1}^s$ is the electrical force at the interface 1–2 (jump of stress). In Eq. 11, $\bar{\mu}_3 \frac{\partial \bar{u}_3}{\partial \bar{y}}$ is the shear stress of fluid 3 at the interface 2–3; $\bar{\mu}_2 \frac{\partial \bar{u}_2}{\partial \bar{y}}$ is the shear stress of fluid 2 at the interface 3–2; M_3 is the dimensionless electrical force at interface 2–3; $\bar{\rho}_{q3}^s$ is the dimensionless density of surface charge, the value can be calculated according interface zeta potential (Gao et al. 2007; Li et al. 2009); $M_3 \bar{\rho}_{q3}^s$ is the electrical force at the interface 2–3 with a jump of stress.

Due to linearity, the velocity of the conducting fluids and of the non-conducting fluid can be decomposed into two parts:

$$\bar{u} = \bar{u}^p + \bar{u}^E \tag{12}$$

where \bar{u}^E corresponds to the velocity driven by electroosmotic force, and \bar{u}^p is the velocity driven by pressure gradient. With the known velocity distributions of \bar{u}^E and \bar{u}^p , the dimensionless flow rates can be calculated by integrating the velocity distribution, the superscript E represents the electroosmotic effect, while the superscript p represents the hydrodynamic effect. The flow rates q can be determined by integrating across the cross-section of the streams:

$$\bar{q}_1^E = 2 \int_{-\bar{h}}^{-\bar{h}-\bar{h}_1} \int_0^{\bar{w}} \bar{u}_1^E(\bar{y}, \bar{z}) d\bar{z} d\bar{y} \tag{13}$$

$$\bar{q}_1^p = 2 \int_{-\bar{h}-\bar{h}_1}^{-\bar{h}} \int_0^{\bar{w}} \bar{u}_1^p(\bar{y}, \bar{z}) d\bar{z} d\bar{y} \tag{14}$$

$$\bar{q}_2^E = 2 \int_{-\bar{h}}^{\bar{h}} \int_0^{\bar{w}} \bar{u}_2^E(\bar{y}, \bar{z}) d\bar{z} d\bar{y} \tag{15}$$

$$\bar{q}_2^p = 2 \int_{-\bar{h}}^{\bar{h}} \int_0^{\bar{w}} \bar{u}_2^p(\bar{y}, \bar{z}) d\bar{z} d\bar{y} \tag{16}$$

$$\bar{q}_3^E = 2 \int_{\bar{h}}^{\bar{h}+\bar{h}_3} \int_0^{\bar{w}} \bar{u}_3^E(\bar{y}, \bar{z}) d\bar{z} d\bar{y} \tag{17}$$

$$\bar{q}_3^p = 2 \int_{\bar{h}}^{\bar{h}+\bar{h}_3} \int_0^{\bar{w}} \bar{u}_3^p(\bar{y}, \bar{z}) d\bar{z} d\bar{y} \tag{18}$$

The analytical solutions of three fluids flow driven by electroosmotic effect and pressure gradient are obtained. The flow rates of the three fluids are functions of the liquid fractions and pressure gradient, $d\bar{p}/d\bar{x}$

$$\begin{cases} \bar{q}_1 = \bar{q}_1(e_1, e_2, e_3, d\bar{p}/d\bar{x}) \\ \bar{q}_2 = \bar{q}_2(e_1, e_2, e_3, d\bar{p}/d\bar{x}) \\ \bar{q}_3 = \bar{q}_3(e_1, e_2, e_3, d\bar{p}/d\bar{x}) \\ e_1 + e_2 + e_3 = 1 \end{cases} \quad (19)$$

where $e_1 = h_1/(h_1 + 2h + h_3)$, $e_2 = 2h/(h_1 + 2h + h_3)$, and $e_3 = h_3/(h_1 + 2h + h_3)$ are the liquid fractions. If the flow rate conditions are specified, the system of equations can be solved numerically using the Newton–Raphson method to determine the liquid fractions and pressure gradient as following process:

- (1) The initial values of e_i are assumed;
- (2) According the initial values of e_i the electroosmotic flow rates of \bar{q}^E for different flows are calculated using Eqs. 13, 15, and 17;
- (3) According the relationship of $\bar{q} = \bar{q}^p + \bar{q}^E$, the pressure-driven flow rates of \bar{q}^p are calculated;
- (4) According the equation of $(d\bar{p}/d\bar{x})_i = (\frac{d\bar{p}}{d\bar{x}})_i(\bar{q}_i^p, e_1, e_2, e_3)$, the values of $(d\bar{p}/d\bar{x})_i$ are calculated;
- (5) Compare the values of $(d\bar{p}/d\bar{x})_i$; if they are same, the values of e_i are the fractions of flows; if they are different, modify the values of e_i . Using the modified values of e_i , repeat steps (2)–(5) until $(d\bar{p}/d\bar{x})_i$ have the same value.

3 Experiments

3.1 Design and fabrication of test devices

Figure 2a shows the layout and the detailed geometries of the microchannels used in our experiments. The test section is a simple straight channel with five output ports. All structures have the same depth of 50 μm . The width of the inlet channel and outlet channel are 0.17 and 0.1 mm, respectively. Two sheath streams are injected into the microchannel from the inlet ports of I_1 and I_3 , the sample stream is injected into the microchannel from the inlet port of I_2 . The sample stream are focused and delivered to the desired outlet ports, Fig. 2b.

Soft lithography technique was used to fabricate the microchannel in PDMS (Nguyen 2006). The layout shown in Fig. 2a is designed using AutoCAD and printed on a transparency film using a laser printer with a resolution of 8000 dpi. The mask design software can realize curved channels. Thus, we used angular channels for the experiments as shown in Fig. 2. A 50- μm thick SU-8 layer was

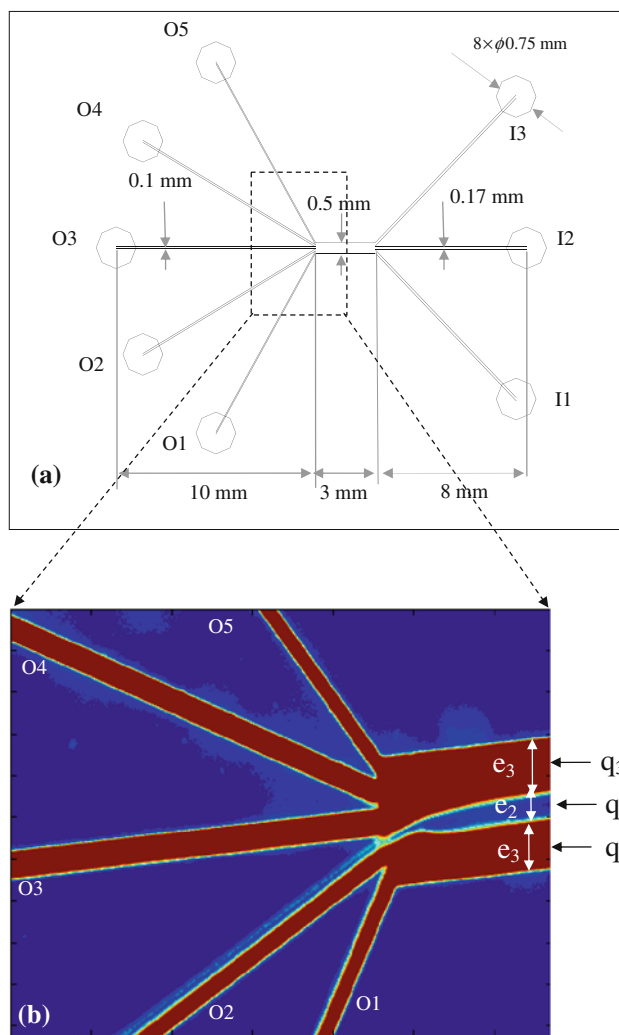


Fig. 2 Flow switching: **a** layout of the PDMS microchannel; **b** measured result of three-fluid electroosmotic flow switching (color online)

first spin-coated on a silicon wafer after soft bake (65°C, 30 min) and hard bake (95°C, 5 min), the SU-8 layer was exposed and developed. The SU-8 master mold was washed in DI water and IPA, and then dried in an oven. PDMS (Dow Corning Corporation, USA) was mixed from the two components (base and curing agent) with a weight ratio of 10:1. The mixed PDMS was placed in a vacuum oven for 20 min to remove air bubbles. The bubble-free PDMS mixture was poured into the SU-8 mold. The PDMS part was then kept at room temperature for 36 h to cure. Subsequently, the cured PDMS was peeled off from the master mold. Eight ports with a diameter of 0.75 mm were punched into the PDMS part. Finally, another cured flat PDMS slab and the PDMS with the microchannels were treated by oxygen plasma and bonded together.

The main problem of a PDMS device is swelling when exposed to silicone oil. For the long duration of the

experiments of droplet switching, PDMS is not suitable as a substrate material. Therefore, PMMA was used as the device material for the droplet switching device. Two PMMA plates were cut by laser-machining and thermally bonded. The laser machined structures were designed by the software of Corel DRAW. The width of the channel is controlled by the width of the drawn lines. The depth of the microchannel can be controlled by the power and speed of the laser beam. The thermal bonding process was achieved using a hot press (CARVER manual press 4386). First, the temperature of the hot plate increases to 165°C. Second, the temperature is kept at 165°C for 30 min. Third, the temperature is reduced to 80°C. Fourth, the temperature is kept at 80°C for 30 min. Finally, the whole system is allowed to cool down to the room temperature. Figure 3a shows the layout and the detailed geometries of the microchannel used in our experiments. They are similar with the previous works (Wang et al. 2005; Li et al. 2009). The test section includes a T-junction channel and a simple straight channel with five output ports. All structures have the same depth of 50 μm . According to the experiments, the curved channel is of advantage for a stable flow especially if the viscosity of the fluid is high.

3.2 Materials

In the experiments of valveless flow switching, de-ionized (DI) water (Millipak[®] Express, Millipore, 0.22 μm) and silicone oil (Sigma–Aldrich) work as sheath streams and sample stream, respectively. Rhodamine B ($\text{C}_{28}\text{H}_{31}\text{N}_2\text{O}_3\text{Cl}$) (Sigma–Aldrich) was added to the DI water as the fluorescent dye to achieve a distinct interface with fluorescent microscopy. The concentration of the fluorescence is 1 g/l. NaCl was diluted in DI water with a concentration of 7×10^{-4} M. The conductivity and viscosity of the NaCl solution are 86.6 $\mu\text{S}/\text{cm}$ and 0.85×10^{-3} Nsm^{-2} , respectively. The viscosity of silicone oil as sample stream is 4.565×10^{-3} Nsm^{-2} . The details of the flow conditions are shown in Table 1.

In the experiments of droplet switching, de-ionized (DI) water was used to form liquid droplets at a T-junction by a continuous mineral oil stream with 2% w/w surfactant Span 80 (Sigma–Aldrich). In order to display the droplets, Rhodamine B was added to the DI water. The concentration of the fluorescence is 1 g/l. The continuous fluid is mineral oil (Sigma–Aldrich). Glycerol was mixed with DI water ($V_{\text{glycerol}}/(V_{\text{DI water}} + V_{\text{glycerol}}) = 0.72$) as sheath streams. NaCl was diluted in aqueous glycerol with a concentration of 7×10^{-4} M. The conductivity and viscosity of the NaCl solution are 86.6 $\mu\text{S}/\text{cm}$ and 2.6×10^{-2} Nsm^{-2} , respectively. The viscosity of mineral oil is 2.69×10^{-2} Nsm^{-2} .

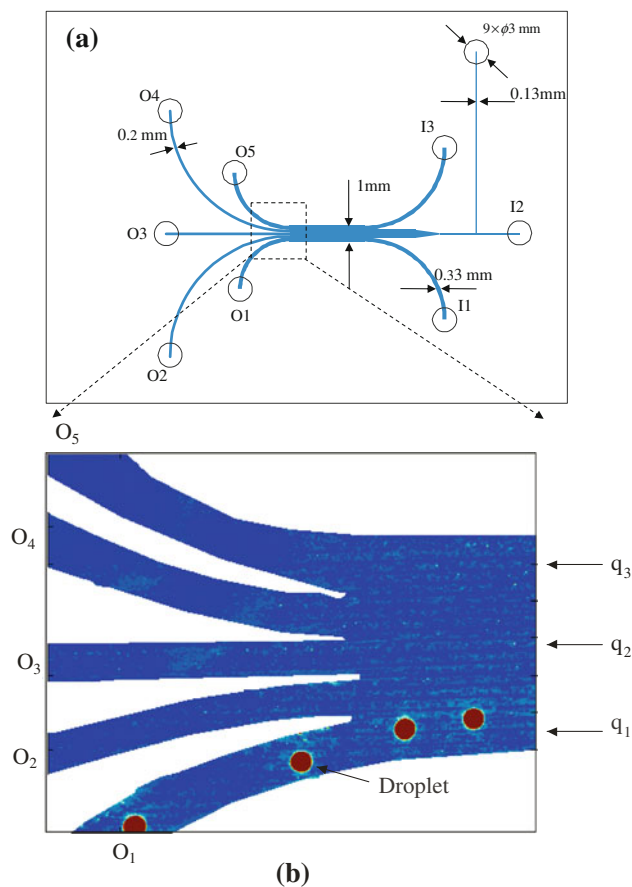


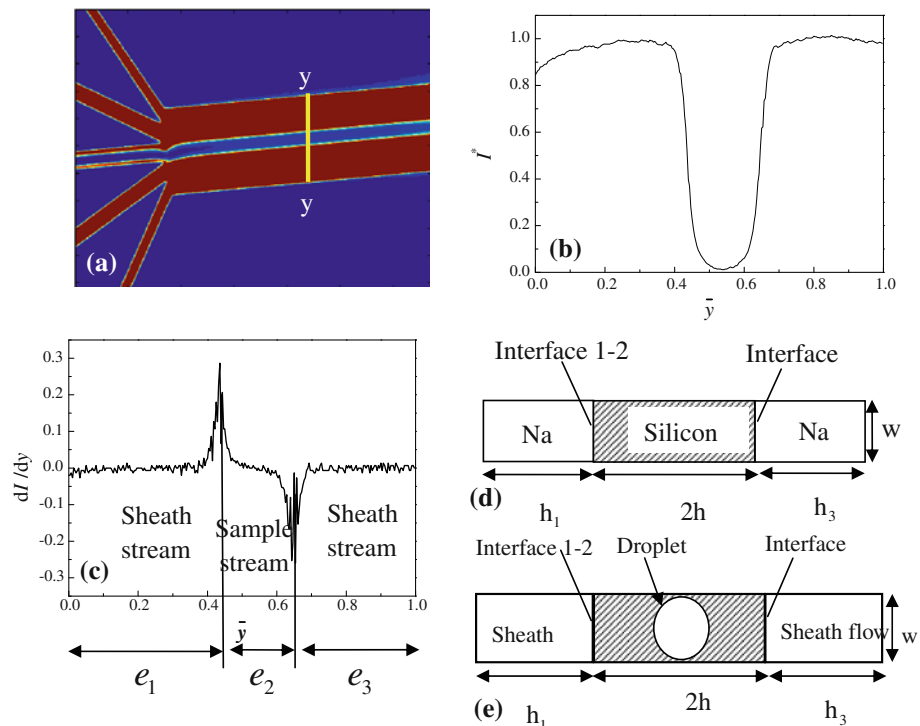
Fig. 3 Droplet switching: **a** layout of the PMMA microchannel for droplet switching; **b** measured result (color online)

3.3 Experimental setup

The experimental setup is shown in Fig. 4. The sheath streams and sample stream were kept in three identical glass syringes (5 ml gastight, Hamilton). Each syringe was pushed by an individual syringe pump (KDS230, KD Scientific Inc, USA, 0.2 $\mu\text{l}/\text{h}$ to 500 l/h, accuracy of 0.5%). In the experiment, the flow rates of three flows were kept constant. The syringes were connected with the inlet ports using hard Teflon tubes. Stainless steel needles (EFD, 5123PC-B, USA) were used to connect the inlet port with the hard Teflon tube. The inner and outer surfaces of the tips were covered with polytetrafluoroethylene. The inner diameter and the outer diameters of the needle are 0.33 and 0.64 mm, respectively. The needles were press fit into the access holes which was previously punched into the PDMS substrate.

Platinum wires (Sigma–Aldrich, 0.1 mm diameter) were used as electrodes, which are inserted into I_1 and O_1 (electric field 1), I_3 and O_5 (electric field 3) from the bottom structure of the PDMS microchannel. The other ports (I_2 , O_2 , O_3 , and O_4) do not have electrodes. Different

Fig. 5 Process of defining the liquid fraction: **a** The location (y - \bar{y}) of the measurement; **b** normalized concentration distribution of the fluorescent dye across the channel width; **c** liquid fractions of the three flows; **d** cross-sectional view of the three fluids in the main channel; **e** cross-sectional view of the switching droplets system in the main channel



cancels the noise in the collected images with an adaptive noise-removal filter. The program also determines the pixel intensity values across the channel, which is normalized using $I^* = (I - I_{\min}) / (I_{\max} - I_{\min})$, where I , I_{\max} , and I_{\min} are the intensity values, its maximum and minimum, respectively. The program calculates the position (y) based on the derivative of concentration (I) with respect to the distance y , can be taken by the formula of $(I_2^* - I_1^*) / (y_2 - y_1)$. The interface position is determined when dI^*/dy is at its maximum value, Fig. 5.

Figure 5d shows the cross-sectional view of the three fluids in the microchannel, h_1 , $2h$, and h_3 are denoted as the width of sheath flow, sample stream, and sheath flow, respectively. Figure 5e shows the cross-sectional view of the channel for droplet switching.

4 Results and discussion

4.1 Switching and focusing under electroosmotic effect

Figure 6 shows a series of pictures for sample stream injection into specific outlet ports. The electroosmotic effect for switching is confirmed experimentally. The sample stream can be delivered into any desired output ports under the coupled effect of hydrodynamics effect and electroosmosis.

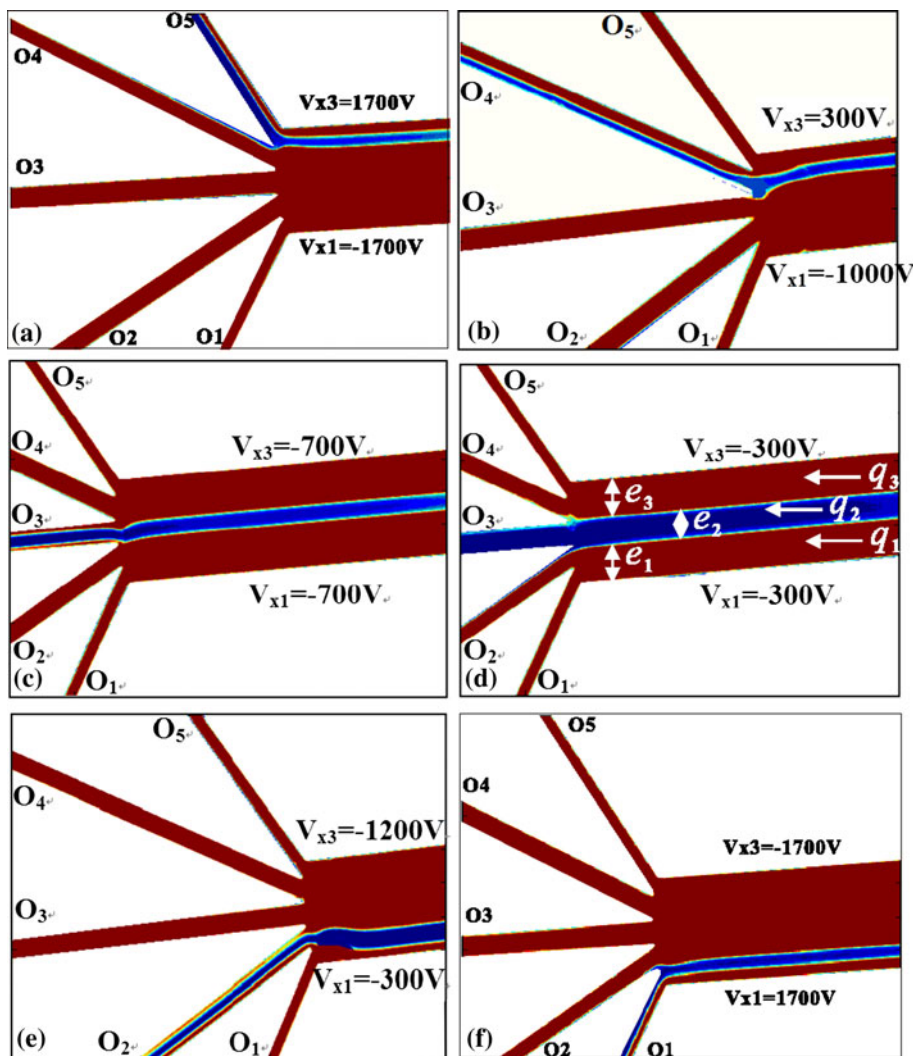
Two sheath streams q_1 and q_3 (conducting liquids of aqueous NaCl), and the sample stream q_2 (silicon oil, dimethylsiloxane 200[®] fluid. Viscosity 5 cSt), are

introduced through the inlets by the syringe pumps. The volumetric flow rate of sample stream (q_2) is 0.1 ml/h, and the volumetric flow rates of sheath flow (q_1 and q_3) are 0.3 ml/h. The mean velocity (U) of the sample stream is about 0.003 m/s. The surface tension (γ) of silicon oil/DI water is 19.7 mN/m, and the capillary number $Ca \approx 7 \times 10^{-4}$. These immiscible fluids flow side by side in a straight rectangular microchannel.

Figure 6a–f shows that at fixed flow rates, the sample stream can be delivered to the desired outlet ports according to the magnitude and the polarity of the electric fields. The results also show that when $V_{x1} = V_{x3}$, the sample stream cannot be switched to other ports except the center port, O_3 . When the magnitudes or polarities of applied two electric fields are different ($V_{x1} \neq V_{x3}$), the droplets are shifted away from the center port.

When a negative electric field is applied along the conducting sheath stream 1 (q_1 , Fig. 6a, $V_{x1} = -1700$ V), the electroosmotic flows act against the pressure-driven flow. Consequently, q_1 encounters a larger resistance and appears to be more “viscous” due to the additional electroosmotic effect. Because the same pressure drop along the microchannel and the fixed volumetric flow rate forced by the syringe pump, the more viscous fluid has to spread over a larger area, thus occupy a larger portion (e_1) of the channel. When a positive electric field is applied along the conducting sheath stream 3 (q_3 , Fig. 6a, $V_{x3} = 1700$ V), the electroosmotic effect acted along the pressure-driven flow, and q_3 is dragged in the same direction as the pressure-driven flow. As a result, q_2 flows faster and occupies a

Fig. 6 Flow focusing and switching based on the combined effect of hydrodynamics and electroosmosis (color coded) ($q_1 = q_3 = 0.3$ ml/h; $q_2 = 0.1$ ml/h): **a** $V_{x1} = -1700$ V, $V_{x3} = 1700$ V; **b** $V_{x1} = -1000$ V, $V_{x3} = 300$ V; **c** $V_{x1} = -700$ V, $V_{x3} = -700$ V; **d** $V_{x1} = -300$ V, $V_{x3} = -300$ V; **e** $V_{x1} = 300$ V, $V_{x3} = -1200$ V; **f** $V_{x1} = 1700$ V, $V_{x3} = -1700$ V



smaller width (e_2) of the channel. The results show that when $V_{x1} = V_{x3} = -300$ V (Fig. 6c) and $V_{x1} = V_{x3} = -700$ V (Fig. 6d), the liquid fraction of NaCl increase symmetrically ($e_1 = e_3$), and the sample stream is delivered to the center port O_3 . The fractions e_1 and e_3 increase with the increase of negative electric fields, hence the focused width e_2 varies with the applied electric fields. In Fig. 6b, when a positive electric field ($V_{x3} = 300$ V) and a negative electric field ($V_{x1} = -1000$ V) are applied, e_3 decrease, and e_1 increase, the sample stream is delivered to port O_4 . Figure 6a, e, f shows that the sample stream can be guided to the desired outlet port by adjusting the magnitude and the polarity of the electric field.

Figure 7 shows that droplets can be delivered to the desired outlet ports according to the magnitude and the polarity of the electric fields. The effect of electric fields is similar to that shown in Fig. 6.

The above results show that a negative electric field could ‘push’ the sample stream (droplet), while a positive electric field could ‘pull’ the sample stream (droplet) in the

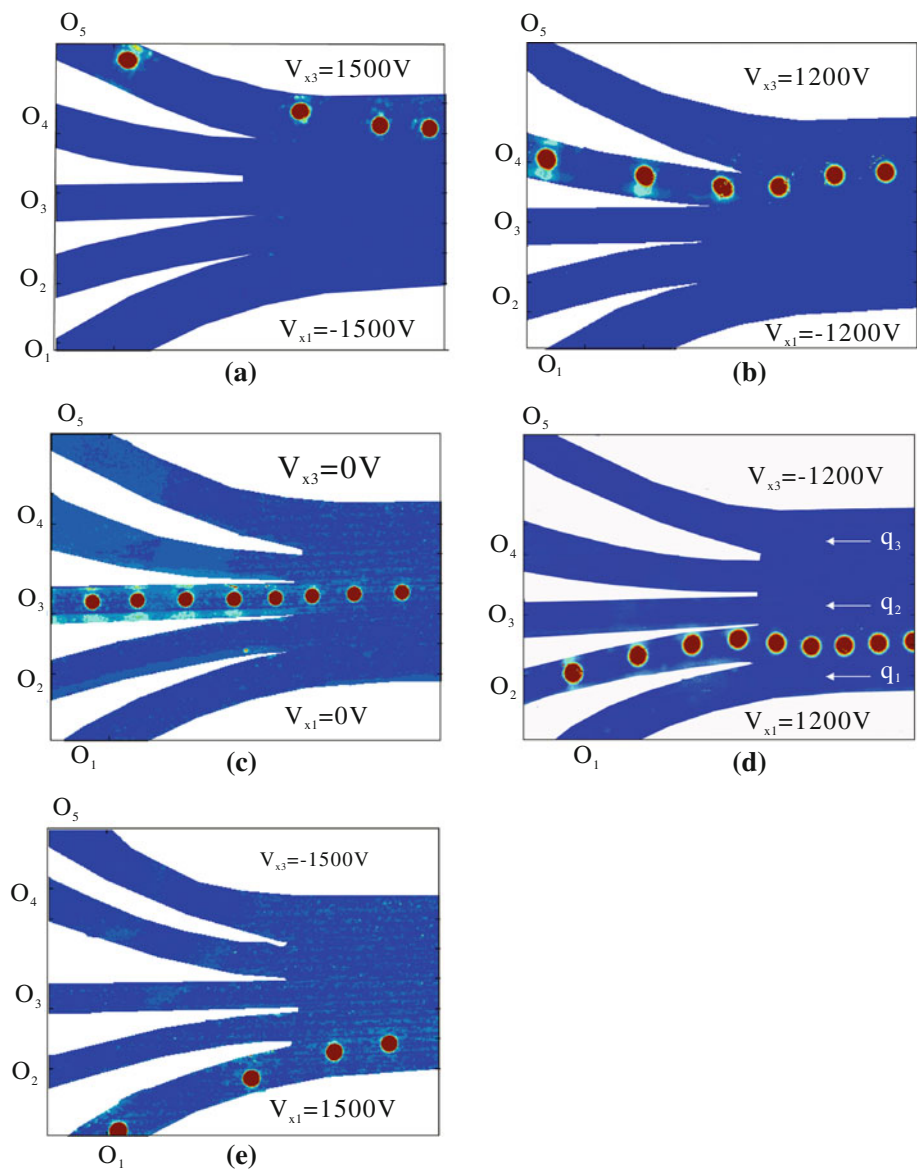
span-wise direction of the microchannel. Hence the position of the interface or of the droplet could be controlled.

4.2 Comparison between theoretical analysis and experiment

Figure 8a compares the measured and mathematical results under different applied electric field strengths. For the mathematical solutions, a reference velocity of $U_{ref} = 1.16 \times 10^{-3}$ m/s, a reference length of $L_{ref} = 500$ μ m, and respective viscosities of NaCl solution and aqueous glycerol of 0.85×10^{-3} and 4.565×10^{-3} Nsm $^{-2}$ were used. The zeta potentials of PDMS and silicon oil with NaCl solution are $\zeta_{PDMS} = -85$ mV(Lee and Li 2006), $\zeta_{oil} = -40$ mV(Gu and Li 1998).

Figure 8a shows the relationship between applied voltages V_{x1} , and V_{x3} for flow switching into desired outlet ports at a fixed flow rates $q_1 = q_3 = 0.3$ ml/h, $q_2 = 0.1$ ml/h. It is clearly seen that the proposed model gives reasonable agreement with the measurement. In general, for guiding the

Fig. 7 Droplet switching based on the combined effects of hydrodynamics and electroosmosis (color coded) ($q_1 = q_2 = q_3 = 0.1$ ml/h): **a** $V_{x1} = -1500$ V, $V_{x3} = 1500$ V; **b** $V_{x1} = -1200$ V, $V_{x3} = 1200$ V; **c** $V_{x1} = 0$ V, $V_{x3} = 0$ V; **d** $V_{x1} = 1200$ V, $V_{x3} = -1200$ V; **e** $V_{x1} = 1500$ V, $V_{x3} = -1500$ V



sample stream into output ports other than the center port, a combination of the positive and negative electric fields is needed. The results further suggest that the most sensitive switching can be achieved by setting the two applied electric fields to have the same magnitude but opposite in polarity, $V_{x1} = -V_{x3}$. This manipulation scheme can be accomplished by using only one high voltage power supply.

Figure 8b shows that the voltage required for flow switching depends on the fluid viscosity ratio. The theoretical results indicated that it is more difficult to switch the sample stream with higher viscosity, because a higher voltage is needed. The switching response becomes slower with the increase of the viscosity of the sample stream.

Figure 9 shows the influence of the applied voltage when $V_{x1} = -V_{x3}$ on the sample stream position in the microchannel. The location of the sample stream for flow switching into desired outlet ports has also been compared

with the analytical model. A rapid increase in the sample stream position occurs when the voltages decrease from 1000 to -1000 V. At fixed flow rates, the switching response under the electroosmotic effect becomes slower as the sample stream is far from the center of the channel.

Experimental results are compared with the analytical results in Figs. 8 and 9. These results agree within a 95% confidence level. The discrepancy between the mathematical model and the experiment is possibly caused by the assumption of flat interfaces and the fluctuation of the pressure gradient provided by the syringe pumps.

5 Conclusions

This paper reports a new technique for switching a non-conducting sample stream or droplets using sheath streams

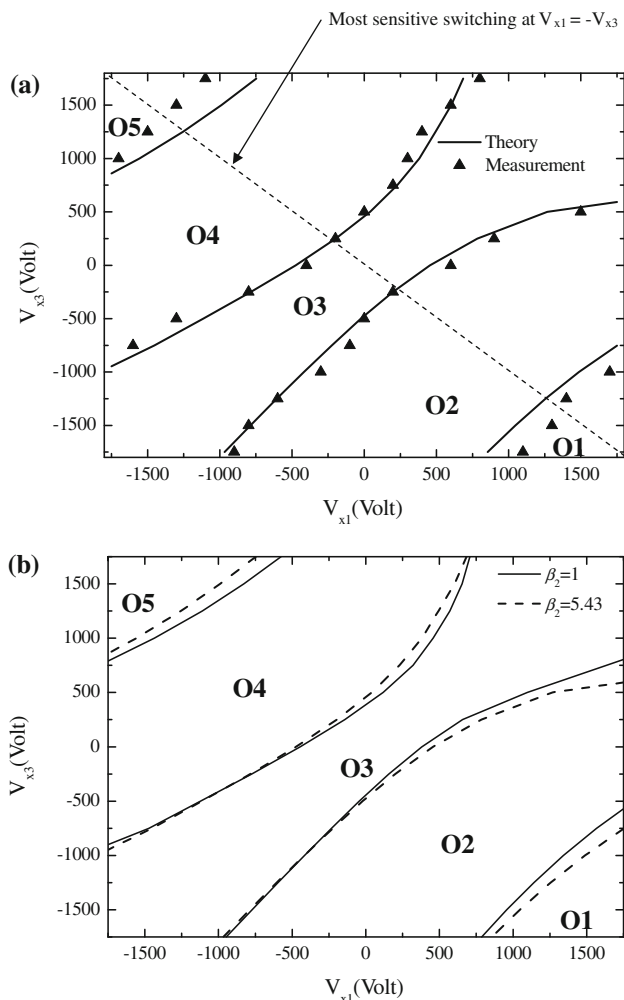


Fig. 8 Relationship between the location of the sample fluid and the applied voltages V_{x1} and V_{x3} ($\beta_1 = \beta_3 = 1$, $q_1 = q_3 = 0.3$ ml/h, $q_2 = 0.1$ ml/h; $\xi_{PDMS} = -85$ mV, $\xi_{oil} = -40$ mV): **a** $\beta_2 = 1$; **b** $\beta_2 = 5.43$

of conducting fluid in a microchannel using the coupled effects of hydrodynamics and electroosmosis. Under the fixed flow rates, the sample stream can be delivered to the desired outlet ports by electroosmosis, rather than the conventional “flow rate ratio” method. By applying different electric fields to the sheath streams along the microchannel, the electroosmotic effect can adjust the velocity of the sheath streams and change the locations of the sample flow. Quantitatively, the liquid fractions and the location of droplets are measured by fluorescence imaging technique. The results indicate that the electric fields can deliver the sample stream to a desired outlet, but two electric fields have to cooperate. The switching speed of about 0.2 s is the only limitation of the presented approach. The comparison of the location of the sample stream between the measured data and the analytical models shows good agreement with a confidence level of 95%.

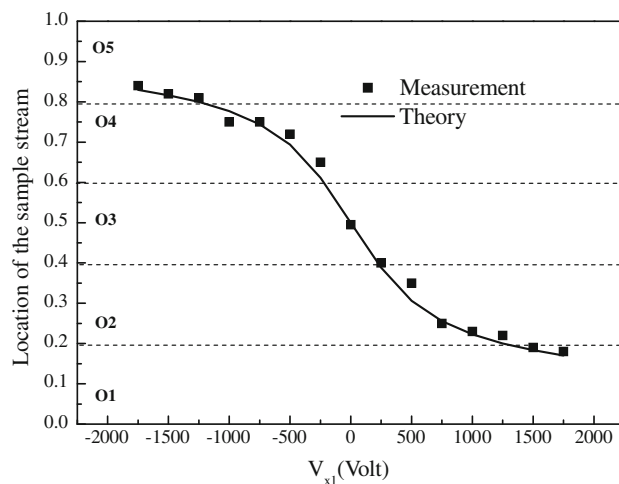


Fig. 9 Relationship between the location of the sample stream and the applied voltages ($\beta_1 = \beta_3 = 1$, $\beta_2 = 5.43$, $q_1 = q_3 = 0.3$ ml/h, $q_2 = 0.1$ ml/h, $V_{x3} = -V_{x1}$, $\xi_{PDMS} = -85$ mV, $\xi_{oil} = -40$ mV)

References

Andersson H, Van den Berg H (2003) Microfluidic devices for cellomics: a review. *Sens Actuators B* 92(3):315–325

Ateya DA, Erickson JS, Howell P B Jr, Hilliard LR, Golden JP, Ligler FS (2008) The good, the bad, and the tiny: a review of microflow cytometry. *Anal Bioanal Chem* 391(5):1485–1498

Besselink GAJ, Vulto P, Lammertink RGH, Schlautmann S, van den Berg A, Olthuis W, Engbers GHM, Schasfoort RBM (2004) Electroosmotic guiding of sample flows in a laminar flow chamber. *Electrophoresis* 25(21–22):3705–3711

Braschler T, Demierre N, Nascimento E, Silva T, Oliva AG, Renaud P (2008) Continuous separation of cells by balanced dielectrophoretic forces at multiple frequencies. *Lab Chip* 8(2): 280–286

Brask A, Goranović G, Jensen MJ, Bruus H (2005) A novel electroosmotic pump design for nonconducting liquids: theoretical analysis of flow rate-pressure characteristics and stability. *J Micromech Microeng* 15(4):883–891

Campbell K, Groisman A, Levy U, Pang L, Mookherjea S, Psaltis D, Fainman Y (2004) A microfluidic 2 × 2 optical switch. *Appl Phys Lett* 85(25):6119–6121

Chen C-H, Santiago JG (2002a) Electrokinetic instability in high concentration gradient microflow. *American Society of Mechanical Engineers. Fluids Engineering Division (Publication) FED* 258, pp 415–418

Chen CH, Santiago JG (2002b) A planar electroosmotic micropump. *J Microelectromech Syst* 11(6):672–683

Chen CH, Lin H, Lele SK, Santiago JG (2005) Convective and absolute electrokinetic instability with conductivity gradients. *J Fluid Mech* 524:263–303

Dittrich PS, Manz A (2005) Single-molecule fluorescence detection in microfluidic channels—the Holy Grail in μ TAS? *Anal Bioanal Chem* 382(8):1771–1782

Dittrich PS, Tachikawa K, Manz A (2006) Micro total analysis systems. Latest advancements and trends. *Anal Chem* 78(12): 3887–3907

Fu LM, Yang RJ, Lee GB, Pan YJ (2003) Multiple injection techniques for microfluidic sample handling. *Electrophoresis* 24(17):3026–3032

- Fu LM, Yang RJ, Lin CH, Pan YJ, Lee GB (2004) Electrokinetically driven micro flow cytometers with integrated fiber optics for on-line cell/particle detection. *Anal Chim Acta* 507(1):163–169
- Gao Y, Wang C, Wong TN, Yang C, Nguyen NT, Ooi KT (2007) Electro-osmotic control of the interface position of two-liquid flow through a microchannel. *J Micromech Microeng* 17(2):358–366
- Gu Y, Li D (1998) The ζ -potential of silicone oil droplets dispersed in aqueous solutions. *J Colloid Interface Sci* 206(1):346–349
- Haiwang L, Wong TN, Nguyen NT (2009) Analytical model of mixed electroosmotic/pressure driven three immiscible fluids in a rectangular microchannel. *Int J Heat Mass Transfer* 52(19–20):4459–4469
- Huh D, Gu W, Kamotani Y, Grotberg JB, Takayama S (2005) Microfluidics for flow cytometric analysis of cells and particles. *Physiol Meas* 26(3):R73–R98
- Huh D, Bahng JH, Ling Y, Wei HH, Kripfgans OD, Fowlkes JB, Grotberg JB, Takayama S (2007) Gravity-driven microfluidic particle sorting device with hydrodynamic separation amplification. *Anal Chem* 79(4):1369–1376
- Kohlheyer D, Besselink GAJ, Lammertink RGH, Schlautmann S, Unnikrishnan S, Schasfoort RBM (2005) Electro-osmotically controllable multi-flow microreactor. *Microfluid Nanofluid* 1(3):242–248
- Lee JSH, Li D (2006) Electroosmotic flow at a liquid-air interface. *Microfluid Nanofluid* 2(4):361–365
- Lee GB, Lin CH, Chang SC (2005) Micromachine-based multi-channel flow cytometers for cell/particle counting and sorting. *J Micromech Microeng* 15(3):447–454
- Li H, Wong TN, Nguyen NT (2009) Electroosmotic control of width and position of liquid streams in hydrodynamic focusing. *Microfluid Nanofluid* 7:489–497
- Lin CH, Lee GB (2003) Micromachined flow cytometers with embedded etched optic fibers for optical detection. *J Micromech Microeng* 13(3):447–453
- Lin H, Storey BD, Oddy MH, Chen CH, Santiago JG (2004) Instability of electrokinetic microchannel flows with conductivity gradients. *Phys Fluids* 16(6):1922–1935
- Maenaka H, Yamada M, Yasuda M, Seki M (2008) Continuous and size-dependent sorting of emulsion droplets using hydrodynamics in pinched microchannels. *Langmuir* 24(8):4405–4410
- McClain MA, Culbertson CT, Jacobson SC, Ramsey JM (2001) Flow cytometry of *Escherichia coli* on microfluidic devices. *Anal Chem* 73(21):5334–5338
- Nguyen NT (2006) Fundamentals and applications of microfluidics. Boston, Artech House
- Nguyen NT, Kong TF, Goh JH, Low CLN (2007) A micro optofluidic splitter and switch based on hydrodynamic spreading. *J Micromech Microeng* 17(11):2169–2174
- Pan YJ, Lin JJ, Luo WJ, Yang RJ (2006) Sample flow switching techniques on microfluidic chips. *Biosens Bioelectron* 21(8):1644–1648
- Pan YJ, Ren CM, Yang RJ (2007) Electrokinetic flow focusing and valveless switching integrated with electrokinetic instability for mixing enhancement. *J Micromech Microeng* 17(4):820–827
- Stone HA, Stroock AD, Ajdari A (2004) Engineering flows in small devices: microfluidics toward a lab-on-a-chip. *Annu Rev Fluid Mech* 36:381–411
- Tan YC, Lee AP (2005) Microfluidic separation of satellite droplets as the basis of a monodispersed micron and submicron emulsification system. *Lab Chip* 5(10):1178–1183
- Taylor JK, Ren CL, Stubbley GD (2008) Numerical and experimental evaluation of microfluidic sorting devices. *Biotechnol Prog* 24(4):981–991
- Wang C, Gao Y, Nguyen NT, Wong TN, Yang C, Ooi KT (2005) Interface control of pressure-driven two-fluid flow in microchannels using electroosmosis. *J Micromech Microeng* 15(12):2289–2297
- Wolfe DB, Conroy RS, Garstecki P, Mayers BT, Fischbach MA, Paul KE, Prentiss M, Whitesides GM (2004) Dynamic control of liquid-core/liquid-cladding optical waveguides. *Proc Natl Acad Sci USA* 101(34):12434–12438
- Wu Z, Nguyen NT (2005) Rapid mixing using two-phase hydraulic focusing in microchannels. *Biomed Microdevices* 7(1):13–20
- Wu Z, Nguyen NT, Huang X (2004) Nonlinear diffusive mixing in microchannels: theory and experiments. *J Micromech Microeng* 14(4):604–611
- Yang RJ, Chang CC, Huang SB, Lee GB (2005) A new focusing model and switching approach for electrokinetic flow inside microchannels. *J Micromech Microeng* 15(11):2141–2148
- Yang SY, Hsiung SK, Hung YC, Chang CM, Liao TL, Lee GB (2006) A cell counting/sorting system incorporated with a microfabricated flow cytometer chip. *Meas Sci Technol* 17(7):2001–2009